Shallow Coastal Water Responses During the Near Landfall Intensification of Tropical Cyclones in the South China Sea

Chunyi Xiang[1, 2], Hironori Fudeyasu[2, 3], Udai Shimada[2, 4], and Ryuji Yoshida[2, 5]

[1]*National Meteorological Center*, *China Meteorological Administration*, *Beijing*, *China*
[2]*Typhoon Science and Technology Research Center*, *Yokohama National University*, *Yokohama*, *Japan*
[3]*Graduate School of Education*, *Yokohama National University*, *Yokohama*, *Japan*
[4]*Meteorological Research Institute*, *Tsukuba*, *Japan*
[5]*Graduate School of Environment and Information Sciences*, *Yokohama National University*, *Yokohama*, *Japan*

(Manuscript received 5 October 2023, accepted 9 January 2024)

Abstract Shallow coastal seawater response during the passage of near-landfall intensification (NLI) tropical cyclones (TCs) and non-NLI TCs was examined using oceanic and atmospheric reanalysis data and observations. The sea surface temperature ahead of the NLI-TC track is maintained or even increases when NLI-TC is approaching the land. The magnitude of the wind stress, which plays an important role in the NLI process, is related to the zonal surface wind on the right side of the tracks. Coastal mixed layer warming can be explained by Ekman transport under sustained wind stress due to surface wind forcing. The successive deepening of the coastal ocean boundary layer and the increase in warming in the subsurface seawater temperature by an average of 0.3°C, could maintain thermal capacity in a certain degree. This shallow coastal water response could partly explain the NLI progress in the northern South China Sea, indicating the importance of coastal ocean dynamics and air-sea interactions.

Citation: Xiang, C., H. Fudeyasu, U. Shimada, and R. Yoshida, 2024: Shallow coastal water responses during the near landfall intensification of tropical cyclones in the South China Sea. *SOLA*, **20**, 55−61, doi:10.2151/sola.2024-008.

1. Introduction

Sudden changes of tropical cyclone (TC) track and intensity, especially the Near-landfall Intensification (NLI), are one of the most challenged problems in TC research and forecasting (Wang and Wu 2004; Emanuel 2018; Tan et al. 2022). Oceanic feedback and air–sea interaction play an important role in TC intensity change (Soloviev et al. 2014; Shay et al. 2000; Lok et al. 2022). Previous studies have highlighted the cooling effect, as cold wakes in the upper ocean, which could suppress TC intensification (Lin et al. 2013; Bender and Ginis 2000; Guo et al. 2020), especially for larger and/or slower-moving TCs (Liu et al. 2023).

Recently, studies have also noted the thermodynamic and dynamic responses in shallow coastal water to NLI-TC as a result of the development of oceanic boundary layer and wind-driven coastal circulation (Liu et al. 2011; Warner et al. 2017). Besides vertical ocean-mixing in the upper ocean, coastal downwelling ahead of TC passage can maintain warm seawater (Gramer et al. 2022) in the studies of Atlantic hurricanes (Miles et al. 2017; Dzwonkowski et al. 2020) and western north Pacific TCs (Zhang et al. 2019; Zhang 2022). In those studies, wind-induced oceanic feedback over the continental shelf played a positive role for TC intensification, which could compensate the cooling effect in the NLI processes (Lok et al. 2022; Pun et al. 2023).

Since the ratio of rapid intensification TCs in the South China Sea (SCS) is comparatively larger than in the western north Pacific (Lei et al. 2022), a comprehensive study of the oceanic feedback in shallow coastal seawater for NLI-TC in SCS is needed. This is meaningful to characterize and quantify the particular air-sea interaction progress during NLI process in SCS with observations.

2. Data and methods

Daily sea surface temperature (SST) data are obtained from the GHRSST (Group for High-Resolution Sea Surface Temperature, https://podaac.jpl.nasa.gov/ghrsst) Version 4.1 (0.01-degree horizontal resolution). Daily oceanic temperature and horizontal velocity during the passage of TC are obtained from the GLORYS (Global Ocean Physics Reanalysis, https://doi.org/10.48670/moi-00021); horizontal resolution is 1/12° and the number of vertical levels is 50. TC intensity, latitude, longitude, and radius of 34 kt wind speed (R34) are derived from the Joint Typhoon Warning Center (JTWC) best tracks (https://metoc.ndbc.noaa.gov/web/guest/jtwc/best_tracks). Current Intensity (CI) number is taken from Advanced Dvorak Technique (ADT) for real-time intensity estimation (Olander and Velden 2019, https://tropic.ssec.wisc.edu/misc/adt/). Surface winds are obtained from ERA5 (the fifth generation ECMWF reanalysis data, Hersbach et al.

Corresponding author: Hironori Fudeyasu, Yokohama National University, 79-2 Tokiwadai, Hodogaya-ku, Yokohama, Kanagawa 240-8501, Japan. E-mail: fude@ynu.ac.jp.

2023), and supplemented by one anchored buoy observation in SCS.

The magnitude of the wind stress (τ_{wind}) is defined as a function of surface wind speed (U), while ρ_{air} (= 1.225 k gm^{-3}) is the density of air and C_d is the drag coefficient (Trenberth et al. 1990),

$$\tau_{\text{wind}} = \rho_{\text{air}} C_d U^2 \tag{1}$$

As the drag coefficient varies under diverse wind forcing, we use the followin g formula to calculate C_d (Hwang et al. 2019),

$$C_d = \begin{cases} (0.8 + 0.065U) * 10^{-3}, & \text{when } U \leq 31.5\ \text{m} \cdot \text{s}^{-1} \\ \left[0.55 + 2.97\left(\dfrac{U}{31.5}\right) - 1.49\left(\dfrac{U}{31.5}\right)^2\right] * 10^{-3}, & \text{when } U \geq 31.5\ \text{m} \cdot \text{s}^{-1} \end{cases} \tag{2}$$

In the coastal region, the vertical integrated temperature provide more information than ocean heat content, which decreases with isobath of sea water (Price 2009). So the depth-integrated temperature T_d is given as follow,

$$T_d(x, y) = \frac{1}{d}\int_d^0 T(x, y, z)dz \tag{3}$$

where d is the isobath in the coastal region. ΔT_d is the daily increasing of T_d from the non-TC status (4 days before landfall) to landfall, with positive values indicate overall warming in the mixed layer.

In order to quantitatively analyze the ocean temperature (T_o) budget, the following three-dimensional equation is used (Jacob et al. 2000; Zhang et al. 2019).

$$\frac{\partial T_o}{\partial t} = -\underbrace{\left(u\frac{\partial T_o}{\partial x} + v\frac{\partial T_o}{\partial y}\right)}_{\text{HADV}} - \underbrace{\omega\frac{\partial T_o}{\partial z}}_{\text{VADV}} + \underbrace{D_t(T_o)}_{\text{HMIX}} + \underbrace{D_z(T_o)}_{\text{VMIX}} + \underbrace{I(Z)}_{\text{FORCE}} \tag{4}$$

where u, v and ω are velocities of seawater. The left side of Eq. (4) is tendency of T_o, while the right terms are horizontal advection (HADV), vertical advection (VADV), horizontal mixing (HMIX), vertical mixing (VMIX) and heat forcing (FORCE) respectively. For VMIX, $D_z(T_o) = \frac{1}{h}\left[k_Z \frac{\partial T_o}{\partial z}\right]_{-h}$, where k_z is the vertical diffusion coefficient (Webb and Suginohara 2001). In this work, the oceanic feedback during the NLI process in terms of HADV and VMIX are mainly discussed, since the HMIX and FORCE are an order of magnitude smaller than the other terms (Zhang et al. 2019).

3. Results

3.1 Near-landfall intensification

In order to exam the air–sea interaction process in the shallow coastal region of the SCS, typical NLI-TCs with remarkable intensification near landfall and non-NLI TCs with similarities in track and landfall point of the same year are selected in three pairs (Fig. 1a). NLI-TC which has over 10 knots of maximum Vmax change within 6 hours and over 1.0 of CI increase, shows significant intensification compared to non-NLI one (Fig. 1b). The translation speeds of NLI-TC are comparatively slower than non-NLI, but with expansion of size (R34) within 24 hours before landfall (Fig. 1c). Vertical wind shear (VWS)[1], as a main atmospheric factor, on the other hand, show little difference. Since the NLI process mainly occurs in the shallow continental shelf region, a target area is defined to quantify oceanic response in the following research (dashed box with four points labeled in Fig. 1a).

3.2 Sea surface responses during the NLI

Daily SST profiles, sliced along the TC track within 24 hours before landfall, of both NLI-TC and non-NLI TC are given respectively (Fig. 2). Consist with previous studies (Zhang et al. 2019; Pu et al. 2019; Lok et al. 2021), the SST cooling occurs during NLI process. Nevertheless, the maximum cooling effect generally happens 1–3 days after TC passage (Dare and McBride 2011), indicating that the SST was not decrease remarkably before landfall. When a NLI-TC moves from P-24hr to P-0hr (within 24 hours before landfall), the SST ahead of its track could inversely warm up rather than cool down. Even if the initial SST differs individually, the near-landfall warming up of sea surface could favor intensification of NLI-TCs.

3.3 Wind stress on coastal seawater

To further distinguish the wind forcing on coastal seawater, the surface wind distributions averaged within 24 h

[1] VWS is calculated based on the 850- and 200-hPa horizontal wind difference, averaged around donuts area (200–800 km) from TC center.

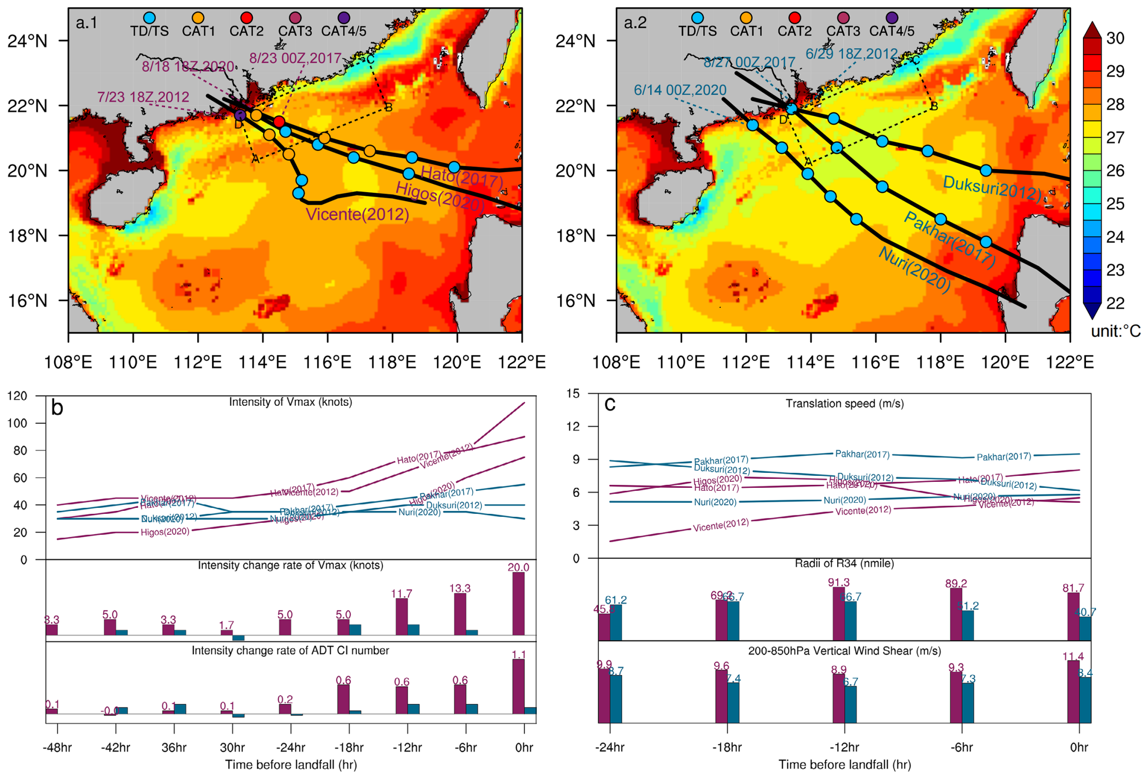

Fig. 1. 0~100 m vertical averaged ocean temperature composited on the day of landfall (shading, °C) for NLI (a.1) and non-NLI (a.2) with track and intensity (circles in color) every 6 hr (the final date before landfall is labeled). The dashed black box (A-D) indicates the shallow continental shelf area in the northern SCS. Comparison of Vmax (knots, b. top), composite of intensity changes rate of Vmax (knot, b. middle) and CI number (b. bottom) every 6 hr of two groups. Comparison of translation speed ($m \cdot s^{-1}$, c. top), composite of radii of R34 (nmile, c. middle) and 200–850 hPa VWS (c. bottom).

before landfall for both NLI-TCs and non-NLI TCs are given (Fig. 3). The overall wind speed of NLI-TCs is correspondingly higher than that of non-NLI TCs; asymmetrically stronger zonal-wind on the right side of their tracks is a characteristic of wind field in NLI-TC. Considering the specific intersection between the SCS coastline and northwestward track, the onshore Ekman transport is sensitive to zonal-wind (Liu et al. 2011). It means that only easterly winds can force coastal downwelling on the right side of tracks. Therefore, only the surface zonal-wind component is used to calculate the wind stress by Eq. (1) in Fig. 4. Besides composited zonal-winds in target area, buoy observations for TCs in 2017 and 2020 are also provided for reference. For NLI-TC, the zonal-wind speed increase dramatically within the 24 h before landfall (Fig. 4a). Meanwhile, the composite wind stress over coastal seawater of NLI-TC is three times more than that of non-NLL TC (with maximum wind stress up to 0.9 $N \cdot m^{-2}$).

Normally, wind stress can generate Ekman transport with thermal and momentum fluxes in the ocean (Duhart and Straub 2006). In the coastal region, offshore and onshore currents can transport energy and mass by coastal upwelling and downwelling respectively (Zhang et al. 2019; Gramer et al. 2022).

3.4 Seawater responses during NLI

Three-dimensional ocean temperature budget as in Eq. (4) is used to diagnose seawater responds progress under coastal Ekman transport. The results shows that the temperature tendency of NLI-TC has a warming in coastal seawater, with an increase of 0.3°C per day (Fig. 5a1). The HADV shows warm advection and relative cold advection beneath (Fig. 5b1), which might be related to the onshore movement in mixed layer. Due to consistent onshore movement induced by Ekman transport, the coastal downwelling could contribute positive VADV to the bottom of shallow seawater, which compensate the HADV loss. Although VMIX is important term in the open ocean, however the cooling due to vertical mixing show little impact on the target area (Fig. 5c1). In contrast, under weaker wind stress by non-NLI TCs (Figs. 3d–f), the area of positive HADV is limited (Fig. 5b2).

3.5 Coastal boundary layer responses during NLI

As the isobath in the shallow continental shelf decreases dramatically within 250 km from the coastline in the SCS, the depth-integrated temperature T_d in the coastal mixed layer could be used to measure coastal seawater heat flux (Price 2009; Pun et al. 2023). If the density profile is divided into the mixed layer (ML) and the barrier layer (BL), the

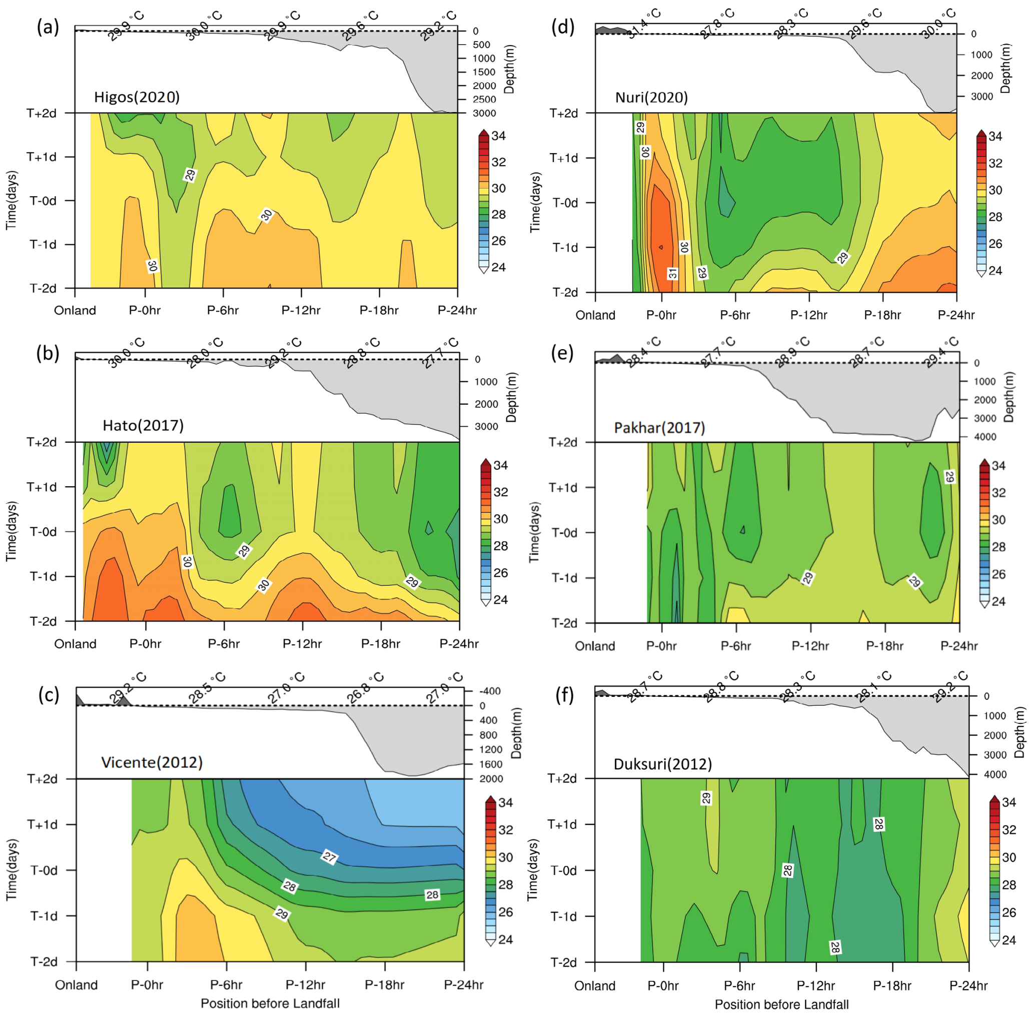

Fig. 2. SST variation (shading; units, °C; 2 days before landfall until 2 days after landfall) during the passage of NLI TCs (a) Higos (2020), (b) Hato (2017), and (c) Vicente (2012) and non-NLI TCs (d) Nuri (2020), (e) Pakhar (2017), and (f) Duksuri (2012) from the TC position 24 h before landfall (P-24hr) to on-land with the ocean bathymetry (units: m) and SST at each position labeled on the top.

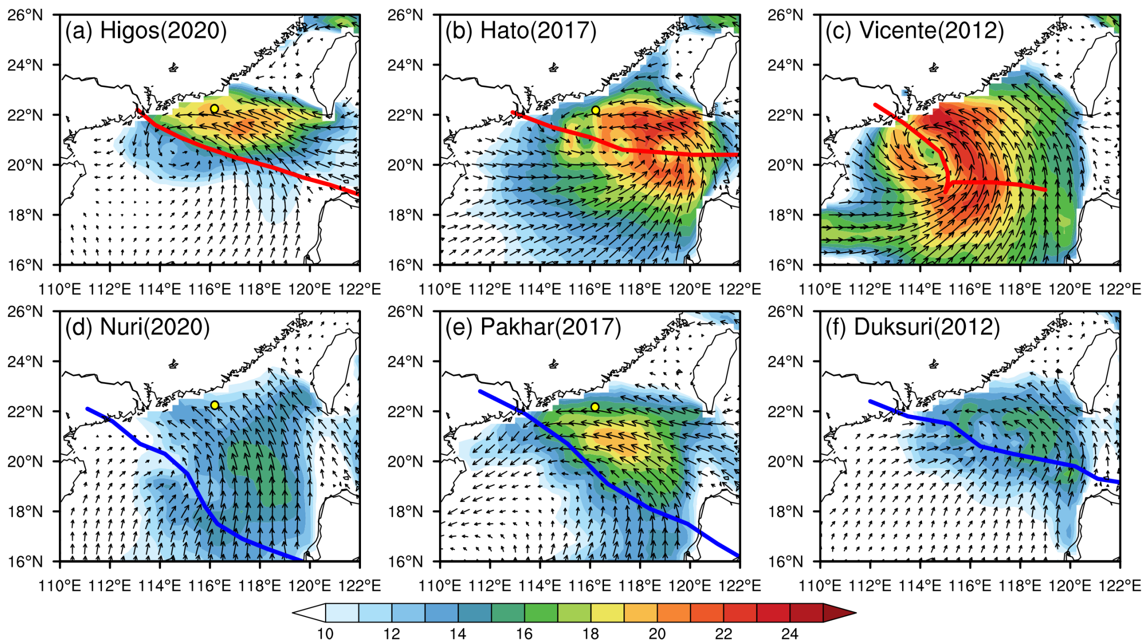

Fig. 3. Surface wind distribution (shading, units, $m{\cdot}s^{-1}$) for the NLI TCs (a) Higos, (b) Hato and (c) Vicente and non-NLI TCs (d) Nuri, (e) Pakhar and (f) Duksuri, with red (blue) lines representing track segments. The yellow circles denote the location of buoy.

temperature evolution averaged in these two layers can be given in Fig. 6 respectively. BL, the layer between the base of ML and the top of the thermocline, acts as a barrier to turbulent entrainment of cooler thermocline seawater into ML and thereby plays an important role on ocean heat budget (Lukas and Lindstrom 1991).

Given the cooling effect induced by vertical mixing and surface fresh water, the NLI-TC experiences a weak cooling in ML, whereas undergoes much stronger warming in BL with the deepening of ML correspondingly (Figs. 6a–6c). The warming of BL can enhance the potential to maintain warm seawater in the coastal region and inhibit the upwelling of cold water (Zhang et al. 2019). Furthermore, the vertical temperature profile of NLI-TC shows that there is a unified warming tendency in BL and cooling in ML indicating that the coastal downwelling might contribute to the positive ΔT_d (Figs. 6d–6f).

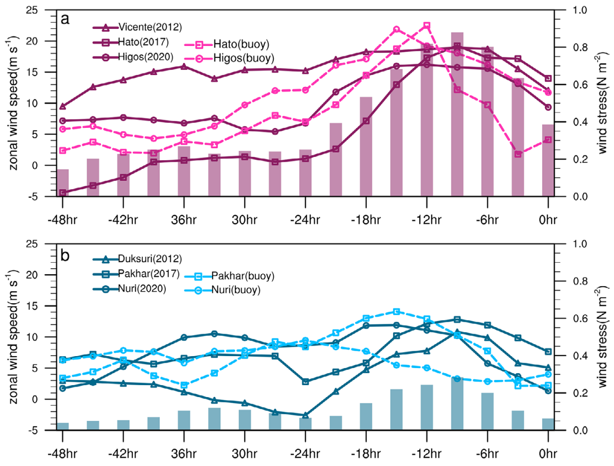

Fig. 4. Surface zonal wind speed evolution (lines, m·s^{-1}, positive indicate eastward winds, with buoy observation dashed, the location of buoy as in Fig. 3d) evolution and composite wind stress (bars, N·m^{-2}) of the zonal wind averaged in the target area in Fig. 1a for the (a) NLI and (b) non-NLI TCs.

4. Conclusion and summary

This paper illustrates the response of shallow coastal water to NLI-TC in the northern SCS. The results shows that coastal subsurface warming and downwelling are related to the wind stress caused by zonal winds to the right of the track when a NLI-TC approaches the land (Fig. 7a). The shallow coastal seawater can warm along the inner-shelf due to coastal downwelling and deepening of the coastal ML, in contrast to the general cooling effect that occurs in the open ocean, where Ekman pumping and vertical mixing can bring cold deep seawater to the surface (Fig. 7b). Onshore current and according coastal downwelling could suppress the loss of warm seawater along the coastline. On average, the coastal seawater temperature increases by 0.3°C, with substantial warming observed in the subsurface. The thermal and dynamical process during the air–sea interaction for NLI TC in the shallow continental shelf will be further discussed by numerical simulation in the future.

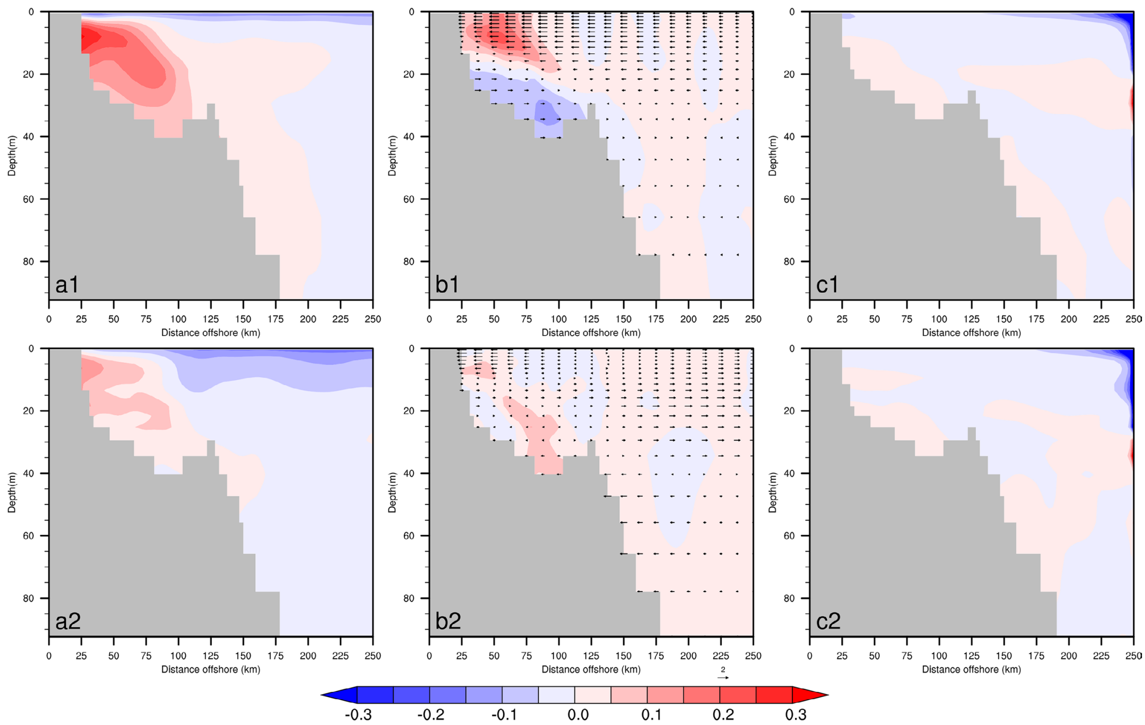

Fig. 5. Depth across-slope section of the temperature tendency (a, shading, °C/day), HADV (b, °C/day) with horizontal velocity (vectors, cm/day) and VMIX (c, °C/day) in equation (4) for NLI (up) and non-NLI (bottom) TCs. The horizontal coordinate is the distance (km) offshore.

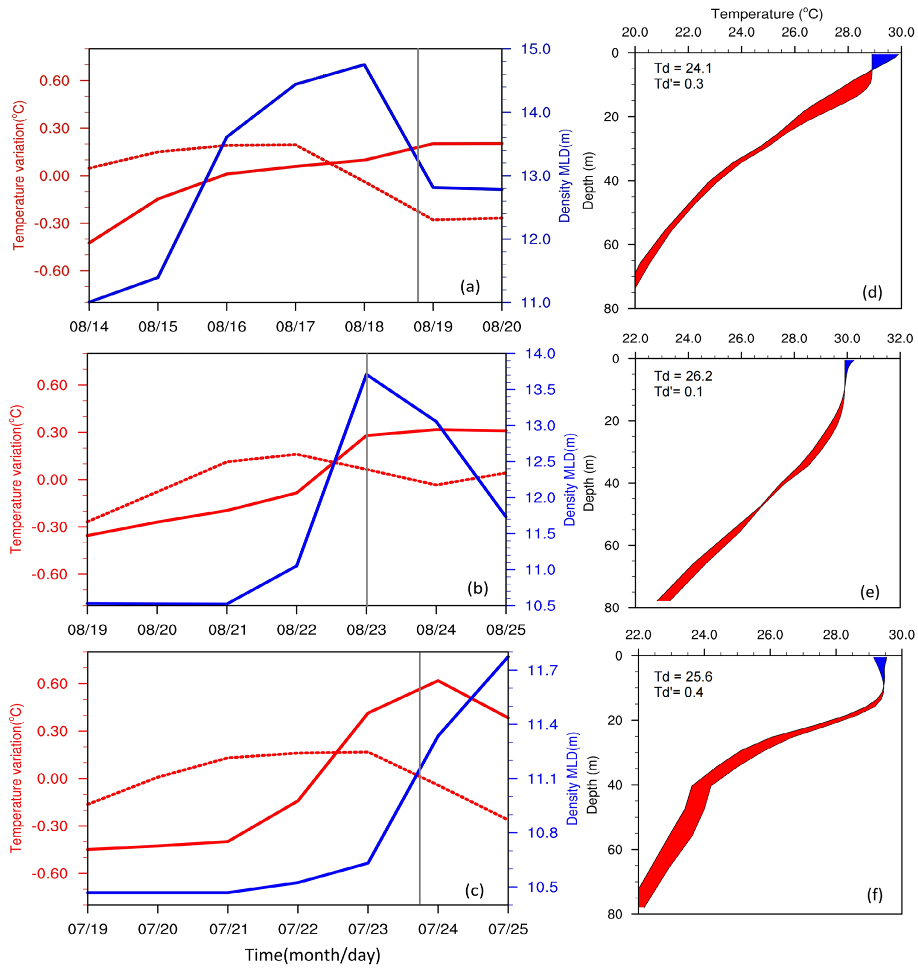

Fig. 6. Evolution of temperature average in the density-defined mixed/barrier layer (red dashed/solid lines, units, °C) and depth of the density defined mixed layer (blue lines, units, m); vertical temperature profile (T_d is depth-integrated temperature to 80 m; ΔT_d is the difference between the non-TC status and landfall) on the right with warming/cooling in red/blue shading.

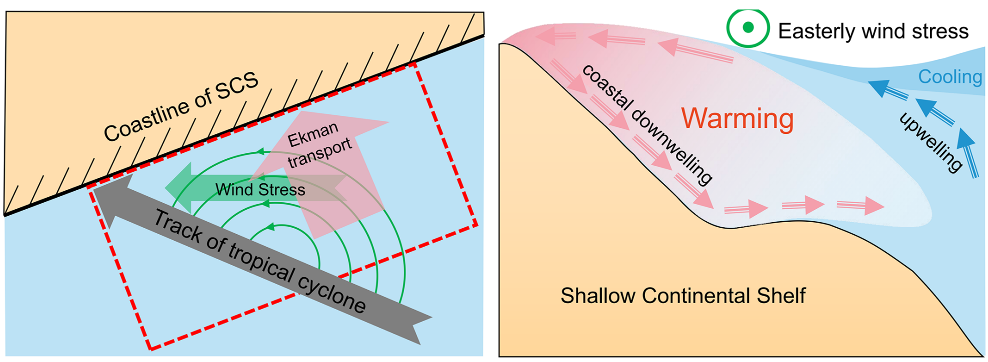

(a) Horizontal conceptual diagram (b) Vertical cross-coastline section conceptual diagram

Fig. 7. Conceptual diagram of (a) horizontal and (b) vertical cross-coastline sections of shallow water responding during the passage of NLI TCs. The red dashed box is the shallow continental shelf area. The gray thick arrow indicates the prevailing track in the SCS. Pink/blue vectors and shadings in (b) denote warming/cooling in the target area shown as the red dashed box of (a).

Acknowledgment

The authors highly appreciate two anonymous reviewers for their pertinent comments and valuable suggestions to help upgrading this study.

Edited by: A. Seiki

References

Bender, M. A., and I. Ginis, 2000: Real-case simulations of hurricane-ocean interaction using a high-resolution coupled model: Effects on hurricane intensity. *Mon. Wea. Rev.*, **128**, 917–946.

Dare, R. A., and J. L. McBride, 2011: Sea surface temperature response to tropical cyclones. *Mon. Wea. Rev.*, **139**, 3798–3808.

Duhart, T. H. A., and D. N. Straub, 2006: Wind stress dependence on ocean surface velocity: Implications for mechanical energy input to ocean circulation. *J. Phys. Oceanogr.*, **36**, 202–211.

Dzwonkowski, B., J. Coogan, S. Fournier, and co-authors, 2020: Compounding impact of severe weather events fuels marine heatwave in the coastal ocean. *Nature Commun.*, **11**, 1–10.

Emanuel, K., 2018: 100 Years of progress in tropical cyclone research. *Meteor. Monogr.*, **59**, 15.1−15.68.

Gramer, L. J., J. A. Zhang, G. Alaka, and co-authors, 2022: Coastal downwelling intensifies landfalling hurricanes. *Geophys. Res. Lett.*, **49**, e2021GL096630.

Guo, T., Y. Sun, L. Liu, and Z. Zhong, 2020: The impact of storm-induced SST cooling on storm size and destructiveness: Results from atmosphere-ocean coupled simulations. *J. Meteor. Res.*, **34**, 1068–1081.

Hersbach, H., B. Bell, P. Berrisford, and co-authors, 2023: ERA5 hourly data on pressure levels from 1940 to present. Copernicus climate Change Service (C3S) Climate Data Store (CDS), doi:10.24381/cds.bd0915c6.

Hwang, P. A., N. Reul, T. Meissner, and co-authors, 2019: Whitecap and wind stress observations by microwave radiometers: Global coverage and extreme conditions. *J. Phys. Oceanogr.*, **49**, 2291–2307.

Yang, L., X. Luo, S. Chen, and co-authors, 2022: Characteristics of rapidly intensifying tropical cyclones in the South China Sea, 1980–2016. *Adv. in Clim. Chan. Res.*, **13**, 333–343,

Lin, I.-I., P. Black, J. F. Price, and co-authors, 2013: An ocean coupling potential intensity index for tropical cyclones. *Geophys. Res. Lett.*, **40**, 1878−1882.

Liu, J., S. Cai, and S. Wang, 2011: Observations of strong near-bottom current after the passage of Typhoon Pabuk in the South China Sea. *J. Mar. Sci.*, **87**, 102–108.

Liu, Y. H., S. D. Guan, I. I. Lin, and co-authors, 2023: Effect of storm size on sea surface cooling and tropical cyclone intensification in the Western North Pacific. *J. Climate*, **36**, 7277–7296.

Lok, C. C. F., J. C. L. Chan, and R. Toumi, 2022: Importance of air-sea coupling in simulating tropical cyclone intensity at landfall. *Adv. Atmos. Sci.*, **39**, 1777−1786.

Lukas, R., and E. Lindstrom, 1991: The mixed layer of the western equatorial Pacific Ocean. *J. Geophys. Res.*, **96**, 3343–3358.

Miles, T., F. Seroka, and S. Glenn, 2017: Coastal ocean circulation during Hurricane Sandy. *J. Geophys. Res. Oceans*, **122**, 7095–7114.

Olander, T. L., and C. S. Velden, 2019: The Advanced Dvorak Technique (ADT) for estimating tropical cyclone intensity: Update and new capabilities. *Wea. Forecasting*, **34**, 905–922.

Price, J. F., 2009: Metrics of hurricane-ocean interaction: Vertically-integrated or vertically averaged ocean temperature? *Ocean Sci.*, **5**, 351–368.

Pun, I. F., H. H. Hsu, I. J. Moon, and co-authors, 2023: Marine heatwave as a supercharger for the strongest typhoon in the East China Sea. *npj Clim. Atmos. Sci.*, **6**, 128.

Shay, L. K., G. J. Goni, and P. G. Black, 2000: Role of a warm ocean feature on Hurricane Opal. *Mon. Wea. Rev.*, **128**, 1366–1383.

Soloviev, A., R. Lukas, M. Donelan, and co-authors, 2014: The air-sea interface and surface stress under tropical cyclones. *Sci. Rep.*, **4**, 5306.

Tan, Z. M., L. L. Lei, Y. Q. Wang, and co-authors, 2022: Typhoon track, intensity, and structure: From theory to prediction. *Adv. Atmos. Sci.*, **39**, 1789−1799.

Trenberth, K. E., W. G. Large, and J. G. Olson, 1990: The mean annual cycle in global ocean wind stress. *J. Phys. Oceanogr.*, **20**, 1742.

Wang, Y., and C. C. Wu, 2004: Current understanding of tropical cyclone structure and intensity changes-A review. *Meteor. Atmos. Phys.*, **87**, 257−278.

Warner, J. C., W. C. Schwab, J. H. List, and co-authors, 2017: Inner-shelf Ocean dynamics and seafloor morphologic changes during Hurricane Sandy. *Cont. Shelf Res.*, **138**, 1–18.

Webb, D. J., and N. Suginohara, 2001: Vertical mixing in the ocean. *Nature*, **409**, 37.

Zhang, H., 2022: Modulation of upper-ocean vertical temperature structure and heat content by a fast-moving tropical cyclone. *J. Phys. Oceanogr.*, **53**, 493–508.

Zhang, Z., Y. Wang, W. Zhang, and J. Xu, 2019: Coastal ocean response and its feedback to Typhoon Hato (2017) over the South China Sea: A numerical study. *J. Geophys. Res.: Atmos.*, **124**, 13731–13749.